Comprehensive insights into effect of van der Waals contact on carbon nanotube network field-effect transistors

Hao Huang, Xingqiang Liu, Fang Liu, Chuansheng Liu, Xuelei Liang, Zhihong Zhang (iD), Kaihui Liu, Xingzhong Zhao, and Lei Liao

View Online   Export Citation   CrossMark

ARTICLES YOU MAY BE INTERESTED IN

Improvement of the electrical performance of $Au/Ti/HfO_2/Ge_{0.9}Sn_{0.1}$ p-MOS capacitors by using interfacial layers
Applied Physics Letters 115, 171601 (2019); https://doi.org/10.1063/1.5121474

Dynamic Q-enhancement in aluminum nitride contour-mode resonators
Applied Physics Letters 115, 173504 (2019); https://doi.org/10.1063/1.5115437

Polycrystalline Co_2Mn-based Heusler thin films with high spin polarization and low magnetic damping
Applied Physics Letters 115, 172401 (2019); https://doi.org/10.1063/1.5121614

Comprehensive insights into effect of van der Waals contact on carbon nanotube network field-effect transistors

Hao Huang,[1] Xingqiang Liu,[2,a)] Fang Liu,[3] Chuansheng Liu,[4] Xuelei Liang,[3] Zhihong Zhang,[5] Kaihui Liu,[5] Xingzhong Zhao,[1,a)] and Lei Liao[1,2,a)]

AFFILIATIONS

[1]School of Physics and Technology, Wuhan University, Wuhan 430072, China
[2]Key Laboratory for Micro-/Nano-Optoelectronic Devices of Ministry of Education, School of Physics and Electronics, Hunan University, Changsha 410082, China
[3]Key Laboratory for the Physics and Chemistry of Nanodevices and Department of Electronics, Peking University, Beijing 100871, China
[4]The Key Laboratory of Artificial Micro- and Nano-Structures, Ministry of Education, School of Physics and Technology, Wuhan University, Wuhan 430072, China
[5]State Key Laboratory for Mesoscopic Physics, School of Physics, Peking University, Beijing 100871, China

[a)]Authors to whom correspondence should be addressed: liuxq@hnu.edu.cn; and xzzhao@whu.edu.cn; liaolei@whu.edu.cn

ABSTRACT

The fermi-level pinning effect caused by low-order contact interface influences the performance of carbon nanotube (CNT) network field-effect transistors (FETs). In this paper, ambipolar CNT network FETs subjected to van der Waals (vdW) contact are demonstrated with the negligible Fermi-level pinning effect by using a physical transfer approach. The vdW contact method allows for the metal and CNT network to retain their intrinsic states without direct chemical bonding and interface interactions, leading to low injection barrier and contact resistance (R_c). Therefore, the field-effect mobilities of vdW metal-semiconductor (MS) contact devices in regions of dominance of the holes (μ_p) and electrons (μ_n) were 18.71 and 2.4 cm^2 V^{-1} s^{-1} and yielded enhancements 2 and 10 times, respectively, beyond those of devices with typically evaporated electrodes. In addition, to develop ambipolar devices with balanced output capability, two-dimensional materials (h-BN and graphene) were inserted into the MS interface to tune the injection barrier. Because the metal work function was effectively reduced by inserting the h-BN layer, devices with h-BN inserted obtained values of μ_p and μ_n of 15.85 and 5.1 cm^2 V^{-1} s^{-1}, respectively. For devices with graphene, because of its field-modulated band alignment capability, μ_n improved to 8.38 cm^2 V^{-1} s^{-1}, while μ_p dropped slightly to 17.5 cm^2 V^{-1} s^{-1}. Therefore, the vdW contact method is a highly efficient integration strategy for high-performance CNT network FETs, and the different insertion layers can efficiently tune the ambipolar transportation of CNT network FETs rather than using different contact metals. This research provides an avenue for the design of future CNT network-based electronics.

Published under license by AIP Publishing. https://doi.org/10.1063/1.5100011

In the past decade, single-walled carbon nanotube (CNT) network field-effect transistors (FETs) have undergone significant development owing to their excellent electrical properties.[1–4] The 2015 ITRS indicates that CNT FETs have the potential to develop the low-power, high-performance electronics in the post-Moore period.[5–8] At the frontier of research on electronics, ambipolar transistors with simplified circuit design and fabrication processes, are gaining increasing attention as an alternative to advanced integrated circuits.[9,10] However, field-effect mobility (μ) values ranging from 0.01 to 55 cm^2 V^{-1} s^{-1} have been obtained in the previously reported CNT network FETs, owing to the different sources of the CNT network and the inconclusive contact properties of the MS interface.[11–14] Inevitable chemical disorder at the MS interface determined by traditional metallization processes usually leads to the Fermi-level pinning effect and therefore severely limits the electrical performance of CNT network FETs.[11,13,15–19] To date, ambipolar CNT network FETs have not been realized via contact engineering.[15–17,20] Therefore, it is important to develop an alternative approach for high-performance ambipolar CNT network electronics.

The van der Waals (vdW) contact strategies are considered as an effective way for implementing high-performance transistors. The transfer-printed metal method was reported to take full advantage of the properties of organic materials.[21] Moreover, the introduced h-BN buffer layer can minimize contact resistance by weakening interactions at the contact interface, whereas the gate-modulated property of graphene enables low injection barriers for both electrons and holes in two-dimensional (2D) material-based transistors.[22–25] Recently, an ideal MS junction associated with the Schottky—Mott rule was experimentally demonstrated for the first time.[26] This can be mainly attributed to the vdW contact which effectively avoids the damage incurred in the evaporation process and diffusion at the contact interface, i.e., the vdW contact strategies can realize an ideal interface without the Fermi-level pinning effect. However, the impact of different kinds of vdW contact on the performance of the CNT network FETs has been rarely reported.

In this paper, high-performance CNT network FETs with three types of vdW contact—Au electrode contact (Tran), Au/graphene electrode contact (Gra), and Au/h-BN electrode contact (Au-BN)—are demonstrated via a simple physical transfer approach.[21,26] Devices with typically evaporated Au electrode contact (Eva) are prepared for comparison. The contact resistance (R_c) of Tran devices is significantly reduced in comparison with that of Eva devices and leads to the enhanced μ of both holes (μ_p from 8.49 to 18.71 cm^2 V^{-1} s^{-1}) and electrons (μ_n from 0.28 to 2.4 cm^2 V^{-1} s^{-1}). Moreover, the inserted h-BN can reduce the effective work function of the metal;[22,25,27] thereafter, Au-BN devices show the increased μ_n from 2.4 to 5.1 cm^2 V^{-1} s^{-1} and the reduced μ_p from 18.71 to 15.85 cm^2 V^{-1} s^{-1}. Benefiting from the tunable Fermi level of graphene,[24] the Gra device exhibits good ambipolar characteristics with μ_p and μ_n of 17.5 and 8.38 cm^2 V^{-1} s^{-1}, respectively, through the gate control. Overall, vdW contact is a highly efficient integration strategy for high-performance CNT network FETs, and Gra devices enable ambipolar CNT network FETs.

The fabrication processes of CNT network FETs with vdW contact are illustrated in Figs. 1(a)–1(f) (for details on the integration of
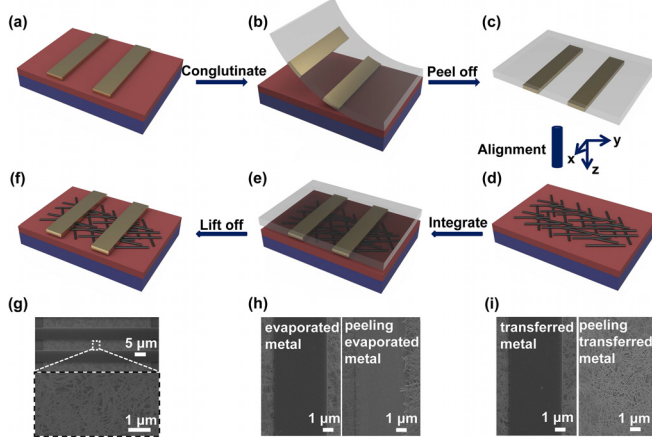
graphene and h-BN layers in the contact regions, see Fig. S1 in the supplementary material). Briefly, 50 nm Au electrodes with/without graphene or an h-BN insertion layer were first prepared on a Si substrate with 300 nm of SiO$_2$ using standard electron beam lithography (EBL) and vacuum evaporation. The Raman shift of graphene is shown in Fig. S2 in the supplementary material and indicates the monolayer graphene. In addition, the h-BN used in this study is identical to that used in the previous work, and the thickness is confirmed to be 1–2 layers.[23] The electrodes are then transferred onto the prepared CNT network on the Si substrate with 300 nm of SiO$_2$ using a polyvinyl alcohol (PVA) film. Finally, de-ionized water is used to lift off the PVA film. Figure 1(g) shows the scanning electron microscope (SEM) image of the CNT network FETs, where the image at the bottom shows the uniform CNT network in the channel area.

To study vdW MS contact beyond the typically evaporated metal contact, the electrodes were mechanically exfoliated from the CNT network after electrical measurement. Figures 1(h) and 1(i) show the SEM image of the typically evaporated contact device and the vdW contact device, respectively. The underlying CNT network is destroyed when the evaporated metal electrodes are mechanically peeled, which can be attributed to the strong chemical bonding of the deposited metal electrodes with the CNT network. By contrast, the underlying CNT network retains its original shape without any apparent damage after peeling the transferred metal electrodes, which suggests weak interaction between the transferred metal electrodes and the CNT network. These results are similar to previous reports demonstrated on the MoS$_2$ system.[26] Clearly, due to the absence of direct chemical bonds at the MS interface, both the metal and the CNT network can maintain their intrinsic states, indicating that vdW MS contact has high-order contact interface and almost no damage to the materials of the channel.

With the optimization of the MS interface, the CNT network FETs with vdW contact exhibited highly tunable characteristics. Figures 2(a) and 2(b) plot the transfer curves ($I_{ds}-V_{gs}$) of the CNT

FIG. 1. (a)–(f) The process flow of the fabrication of vdW MS contact. (g) SEM image of the fabricated CNT network FETs. (h) and (i) SEM image of the typically evaporated contact device and the vdW contact device, respectively. The left and right sides of each figure represent before and after electrodes mechanically released, respectively.
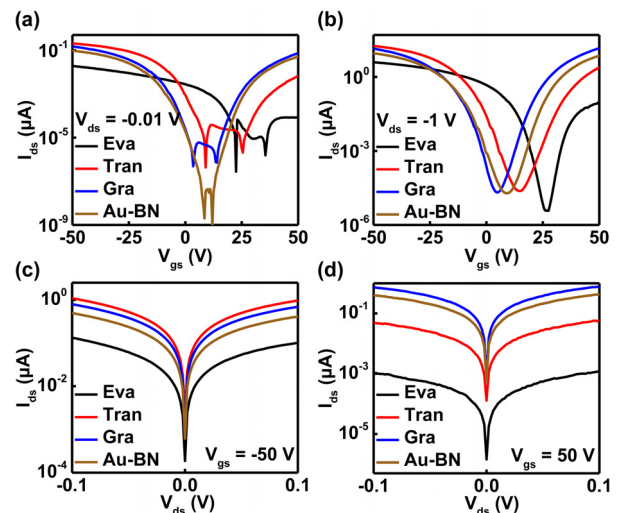
FIG. 2. (a) and (b) The transfer curves ($I_{ds}-V_{gs}$) of CNT network FET with different contact strategies at $V_{ds} = -0.01$ V and -1 V, respectively. (c) and (d) The corresponding output curves of CNT network FET with different contact strategies at $V_{gs} = -50$ V and 50 V, respectively.

network FETs with different contact strategies at $V_{ds} = -0.01$ V and -1 V, respectively. The ON-state currents (I_{ON}) of both the p-branch and the n-branch for the three-type CNT network FETs with the vdW contact significantly increased. Notably, the I_{ON} of Eva devices increases by more than 1000 times with V_{ds} altered from -0.01 to -1 V, indicating that Eva contact introduced a more intense barrier such that I_{ON} was significantly limited at low V_{ds}. To further compare the output current of different types of contact, the corresponding output curves of different CNT network devices under $V_{gs} = -50$ V and 50 V on a semilog scale are shown in Figs. 2(c) and 2(d), respectively. The output curves of different CNT network devices on a linear scale are shown in Fig. S3 in the supplementary material. Specifically, the Tran device had the highest output current at $V_{gs} = -50$ V, whereas the Gra device had the largest output current at $V_{gs} = 50$ V. This means that Tran is the most effective strategy to achieve hole-dominant CNT network FETs, and Gra strategy is suitable for excellent ambipolar CNT network electronics.

Figure 3 shows the reproducibility of the devices with different contact electrodes. Two key electrical parameters of I_{ON} and μ were extracted. I_{ON} was extracted from curves of I_{ds}–V_{gs} with $V_{ds} = -1$ V to intuitively show the conductivity of the channel. Moreover, μ is defined by Eq. (1)

$$\mu = \frac{L}{W} \cdot \frac{G_m}{V_{ds} \cdot C_i}, \qquad (1)$$

where L and W are the channel length and width, respectively; g_m is the transconductance (maximum g_m was used in the calculation of μ for both electrons and holes); and C_i is the gate oxide capacitance per unit area. In the hole-dominated region [Figs. 3(a) and 3(b)], the Tran devices achieved the highest I_{ON}, and the I_{ON} of the Gra devices was slightly larger than that of Au-BN devices. Figure 3(b) indicates that the extracted μ_p values had a similar trend as that of I_{ON}. The average μ_p of devices with vdW contact underwent a significant improvement over that of Eva devices. Specifically, the average μ_p of Tran devices

(18.71 cm^2 V^{-1} s^{-1}) increased by more than 120% compared with that of Eva devices (8.49 cm^2 V^{-1} s^{-1}). In the electron-dominated region [Figs. 3(c) and 3(d)], the I_{ON} of devices with vdW contact increased substantially compared with that of Eva devices. The highest I_{ON} was obtained in Gra devices, whereas the I_{ON} of Tran devices was lower than that of Au-BN devices. The μ_n and I_{ON} of the CNT network FETs also showed trends of positive correlation in the electron-dominated region. Notably, the extracted μ_n of devices with vdW contacts was 10 times larger than that of Eva devices. This can be attributed to the damage-free process and significant weakening of the Fermi-level pinning effect.[21,26] The increase in the μ_n of Au-BN devices occurred mainly because the combination of h-BN and metal effectively reduced the metal work function, and thus, the Schottky barrier height (SBH) in the electron-dominated region of the Au-BN devices was reduced.[25] The gate-tunable band structure of graphene played a key role in the operation of the device,[24] so that the Gra strategy led to low SBH in the electron-dominated region beyond other strategies.

To further quantitatively evaluate the quality of different contact schemes, contact resistance (R_c) was extracted using the transfer length method (TLM).[11,18] CNT network FETs were fabricated on the same CNT network with different channel lengths, as shown in Fig. S4 in the supplementary material. All resistances were obtained at $V_{ds} = -1$ V and $V_{gs} = \pm 50$ V. TLM resistances of devices with different types of contact are plotted in Figs. 4(a) and 4(b), and $2R_c$ was obtained from the intercept of the Y-axis by linear fitting. The extracted R_c is shown in Fig. 4(c). When $V_{gs} = -50$ V, the values of R_c were 3.12, 0.65, 0.77, and 0.84 M$\Omega \cdot \mu$m for Eva, Tran, Gra, and Au-BN devices, respectively. On the contrary, when $V_{gs} = 50$ V, the values of R_c for Eva, Tran, Gra, and Au-BN devices were 268.68, 1.91, 0.84, and 1.29 M$\Omega \cdot \mu$m, respectively. Tran devices had the lowest R_c, nearly five times lower than that of Eva devices at $V_{gs} = -50$ V. Devices with vdW contact recorded more than two orders of magnitude of improvement compared with Eva devices at $V_{gs} = 50$ V, and the
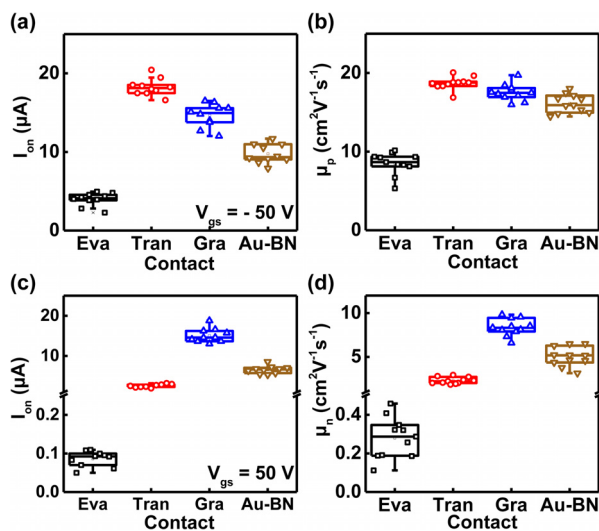
FIG. 3. The statistical I_{ON} and μ of CNT network FETs with different contact strategies at hole-dominated (a) and (b) and electron-dominated regions (c) and (d).
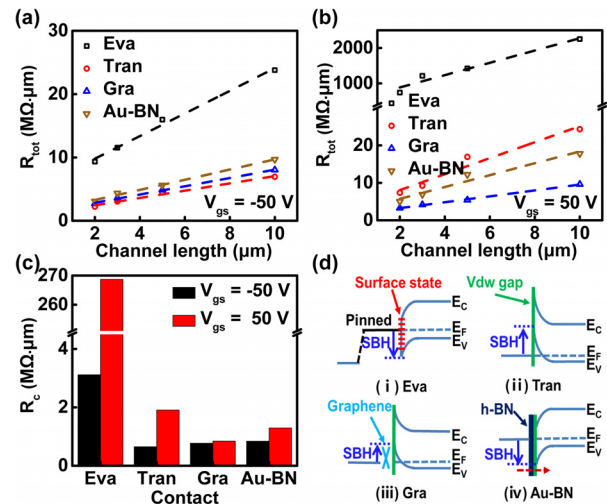
FIG. 4. (a) and (b) TLM resistance of CNT network FETs with different contact strategies at $V_{gs} = -50$ V and 50 V, respectively. (c) The extracted R_c of CNT network FETs with different contact strategies. (d) The energy band diagrams of CNT network FETs for holes with Eva (i), Tran (ii), Gra (iii), and Au-BN (iv).

lowest R_c was observed in Gra devices. All of this indicates that device performance can be readily tuned by vdW contact schemes.

In general, carrier transport at the MS interface can be attributed to thermionic emission, thermionic field emission, and tunneling. Thermionic emission and thermionic field emission currents are significantly influenced by SBH, whereas the tunneling current mainly depends on the thickness of the inserted layer and the vdW gap (negligibly small).[24–26,28,29] Moreover, the SBH is usually positively correlated with R_c and is in accordance with the Schottky–Mott rule in vdW contact.[26,28] The bandgap of the CNT network is usually defined by $0.7/d$, where d is the diameter of the carbon nanotube.[30,31] In this paper, $d = 1.4$ nm. Hence, the bandgap of the CNT film was 0.5 eV. Subsequently, the bandgap of the CNT and the electron affinity of graphite were used to obtain the electron affinities of the CNT network, 4.15 eV.[32,33] The work functions of Au, Au–graphene, and Au-BN were 5.1, 4.79, and 4.53, respectively.[22,23,25] The energy band diagrams of different contact strategies for CNT network FETs are shown in Fig. 4(d). First, for Eva devices [Fig. 4(d-i)], typical processes such as EBL and evaporation usually damage materials, resulting in numerous defects at the interface and the formation of surface state, which causes the Fermi level pinned to the edge of the valence band. As a result, device performance is severely degraded, and electron transport is limited. Second, for Tran devices [Fig. 4(d-ii)], the damage-free process can maintain a perfect contact interface with a small vdW gap. Thus, the effect of Fermi-level pinning is significantly weakened. The initial position of the Fermi level associates with the work function of Au below the maximum of valence band of the CNT network, which means no barrier for holes.[34] Therefore, high hole current was achieved, indicating that Tran is an effective way to achieve unipolar properties for the CNT network. For Gra devices [Fig. 4(d-iii)], apart from a reduction in the effective metal work function, the Fermi level of graphene could be readily tuned by the gate potential; consequently, the devices exhibited excellent ambipolar characteristics and achieved the highest electron current. Note that the initial position of the Fermi-level associates with the effective work function of Gra was also lower than the maximum of the valence band, resulting in no barrier contact for holes.[34] However, compared with Tran devices, the work function of Gra was lower than that of Au and led to lower hole concentration in Gra devices.[34] Therefore, the I_{ON} of the Gra devices was slightly lower than that of Tran devices. Finally, for Au-BN devices [Fig. 4(d-iv)], compared with Tran devices, the enhancement in μ_n and the reduction in μ_p can be attributed to the effective reduction in the metal work function and the introduction of tunneling resistance.[23,25]

In summary, CNT network FETs with vdW contact were systematically investigated in this paper, and the results indicate that vdW contact strategies allow for lower contact resistance as a consequence of weak interface interactions and a negligible Fermi-level pinning effect, thus yielding high-performance CNT network FETs. Compared with conventional Eva devices, Tran devices are superior at hole transport, which can be attributed to the damage-free process that induces a perfect MS interface. The 2D materials inserted at the contact interface also play an important role in device operation to tune the SBH rather than use different metal contacts. Specifically, the h-BN can reduce the effective work function of the metal, sharply increasing μ_n while slightly suppressing μ_p. In addition, the free conversion of hole-dominated and electron-dominated transports of Gra devices with

gate-tunable performance was implemented. With a comprehensive investigation at the contact interface, the results indicate that the vdW contact method is efficient for low contact resistance in CNT network electronics for high-performance applications. Moreover, the gate-tunable property of the inserted graphene layer enables a balanced output current for the fabrication of ambipolar CNT network FETs. Therefore, the work here can provide guidance for the design of future CNT network FETs.

See the supplementary material for the fabrication processes of three types of vdW contacted CNT network FETs, the Raman shift of the CVD grown graphene, the output curve of different contact strategy CNT network devices, and the SEM image of CNT network FETs on the same CNT network with a variable channel length.

REFERENCES

[1] L. Ding, Z. Y. Zhang, S. B. Liang, T. Pei, S. Wang, Y. Li, W. W. Zhou, J. Liu, and L. M. Peng, Nat. Commun. **3**, 677 (2012).
[2] C. A. Wang, J. L. Zhang, and C. W. Zhou, ACS Nano **4**, 7123 (2010).
[3] J. L. Zhang, Y. Fu, C. Wang, P. C. Chen, Z. W. Liu, W. Wei, C. Wu, M. E. Thompson, and C. W. Zhou, Nano Lett. **11**, 4852 (2011).
[4] C. Wang, J. L. Zhang, K. M. Ryu, A. Badmaev, L. G. De Arco, and C. W. Zhou, Nano Lett. **9**, 4285 (2009).
[5] A. D. Franklin, Science **349**, aab2750 (2015).
[6] H. Kawaura, T. Sakamoto, and T. Baba, Appl. Phys. Lett. **76**, 3810 (2000).
[7] M. M. Waldrop, Nature **530**, 144 (2016).
[8] See http://www.itrs2.net/itrs-reports.html for "The International Technology Roadmap for Semiconductors" (last accessed August 1, 2016).
[9] L. Y. Liang, H. T. Cao, X. B. Chen, Z. M. Liu, F. Zhuge, H. Luo, J. Li, Y. C. Lu, and W. Lu, Appl. Phys. Lett. **100**, 263502 (2012).
[10] F. S. Kim, X. Guo, M. D. Watson, and S. A. Jenekhe, Adv. Mater. **22**, 478 (2010).
[11] C. Cao, J. B. Andrews, A. Kumar, and A. D. Franklin, ACS Nano **10**, 5221 (2016).
[12] G. D. Dong, J. Zhao, L. J. Shen, J. Y. Xia, H. Meng, W. H. Yu, Q. Huang, H. Han, X. L. Liang, and L. M. Peng, Nano. Res. **11**, 4356 (2018).
[13] J. Xia, G. Dong, B. Tian, Q. Yan, H. Zhang, X. Liang, and L. Peng, Nanoscale **8**, 9988 (2016).
[14] M. G. Zhu, J. Si, Z. Zhang, and L. M. Peng, Adv. Mater. **30**, e1707068 (2018).
[15] Y. Liu, J. Han, N. Wei, S. Qiu, H. Li, Q. Li, S. Wang, and L. M. Peng, Nanoscale **8**, 17122 (2016).
[16] L. M. Peng, Z. Y. Zhang, S. Wang, and X. L. Liang, AIP Adv. **2**, 041403 (2012).
[17] Z. Y. Zhang, X. L. Liang, S. Wang, K. Yao, Y. F. Hu, Y. Z. Zhu, Q. Chen, W. W. Zhou, Y. Li, Y. G. Yao, J. Zhang, and L. M. Peng, Nano Lett. **7**, 3603 (2007).
[18] J. B. Andrews, K. Mondal, T. V. Neumann, J. A. Cardenas, J. Wang, D. P. Parekh, Y. Lin, P. Ballentine, M. D. Dickey, and A. D. Franklin, ACS Nano **12**, 5482 (2018).
[19] Q. Huang, J. Y. Xia, J. Zhao, G. D. Dong, F. Liu, H. Meng, and X. L. Liang, Sci. Bull. **63**, 802 (2018).
[20] Q. Zeng, S. Wang, L. Yang, Z. Wang, Z. Zhang, L. Peng, W. Zhou, and S. Xie, Nano Res. **5**, 33 (2012).
[21] C. Liu, Y. Xu, Z. Liu, H. N. Tsao, K. Mullen, T. Minari, Y. Y. Noh, and H. Sirringhaus, Org. Electron **15**, 1884 (2014).

[22]M. Farmanbar and G. Brocks, Phys. Rev. B **91**, 161304 (2015).

[23]J. L. Wang, Q. Yao, C. W. Huang, X. M. Zou, L. Liao, S. S. Chen, Z. Y. Fan, K. Zhang, W. Wu, X. H. Xiao, C. Z. Jiang, and W. W. Wu, Adv. Mater. **28**, 8302 (2016).

[24]Y. Liu, H. Wu, H. C. Cheng, S. Yang, E. Zhu, Q. He, M. Ding, D. Li, J. Guo, N. O. Weiss, Y. Huang, and X. Duan, Nano Lett. **15**, 3030 (2015).

[25]M. H. Lee, Y. Cho, K. E. Byun, K. W. Shin, S. G. Nam, C. Kim, H. Kim, S. A. Han, S. W. Kim, H. J. Shin, and S. Park, Nano Lett. **18**, 4878 (2018).

[26]Y. Liu, J. Guo, E. B. Zhu, L. Liao, S. J. Lee, M. N. Ding, I. Shakir, V. Gambin, Y. Huang, and X. F. Duan, Nature **557**, 696 (2018).

[27]J. Su, L. Feng, Y. Zhang, and Z. Liu, Phys. Chem. Chem. Phys. **18**, 16882 (2016).

[28]T. G. Kim, U. J. Kim, S. Y. Lee, Y. H. Lee, Y. S. Yu, S. W. Hwang, and S. Kim, IEEE Trans. Electron Devices **61**, 2203 (2014).

[29]T. Pei, H. T. Xu, Z. Y. Zhang, Z. X. Wang, Y. Liu, Y. Li, S. Wang, and L. M. Peng, Appl. Phys. Lett. **99**, 113102 (2011).

[30]S. Sreekala, X. H. Peng, P. M. Ajayan, and S. K. Nayak, Phys. Rev. B **77**, 155434 (2008).

[31]K. El Shabrawy, K. Maharatna, D. Bagnall, and B. M. Al-Hashimi, IEEE Trans. Nanotechnol. **9**, 184 (2010).

[32]A. Akturk, G. Pennington, and N. Goldsman, IEEE Trans. Electron Devices **52**, 577 (2005).

[33]A. Charlier, R. Setton, and M. F. Charlier, Phys. Rev. B **55**, 15537 (1997).

[34]E. Liu, *The Physics of Semiconductors*, 7th ed. (Publishing House of Electronics Industry, Beijing, 2011), p. 192.